Article

Effect of Substrate Alloy Type on the Microstructure of the Substrate and Deposited Material Interface in Aluminium Wire + Arc Additive Manufacturing

Eloise Eimer [1,*] , Stewart Williams [1], Jialuo Ding [1], Supriyo Ganguly [1] and Bechir Chehab [2]

[1] Welding Engineering and Laser Processing Centre, School of Aerospace, Cranfield University, Transport and Manufacturing, College Road, Cranfield MK43 0AL, UK; s.williams@cranfield.ac.uk (S.W.); jialuo.ding@cranfield.au.uk (J.D.); s.ganguly@cranfield.ac.uk (S.G.)

[2] Constellium Technology Centre, 725 Rue Aristide Berges, 38341 Voreppe, France; bechir.chehab@constellium.com

* Correspondence: e.eimer@cranfield.ac.uk

Abstract: Wire + Arc Additive Manufacture is an Additive Manufacturing process that requires a substrate to initiate the deposition process. In order to reduce material waste, build and lead time, and improve process efficiency, it is desirable to include this substrate in the final part design. This approach is a valid option only if the interface between the substrate and the deposited metal properties conform to the design specifications. The effect of substrate type on the interface microstructure in an aluminium part was investigated. Microstructure and micro-hardness measurements show the effect of substrate alloy and temper on the interface between the substrate and deposited material. Microcracks in the as-deposited condition were only found in one substrate. The deposited material hardness is always lower than the substrate hardness. However, this difference can be minimised by heat treatment and even eliminated when the substrate and wire are made of the same alloy.

1. Introduction

Additive Manufacturing (AM) offers the possibility to reduce production cost and lead time while increasing the shape complexity achievable compared with subtractive manufacturing methods. Wire + Arc Additive Manufacture (WAAM), detailed by Williams et al. [1], is a process suitable for producing large scale components, usually built using conventional manufacturing processes such as machining from wrought parts or forged billets. These large components can be integrated into the primary or secondary structure of an aircraft after a small finishing machining step. WAAM produces 3-D parts by depositing successive layers of material using an electric arc as the heat source and wire as the feedstock.

Aluminium alloys are widely used in aerospace and transport, especially aluminium copper and zinc alloys, well known for their low density, high strength and good damage tolerance. Depending on their compositions, high strength aluminium alloys perform differently, achieving different compromises between static and dynamic mechanical properties. For example, aluminium zinc magnesium copper alloys are used in combination with aluminium copper alloys in aircraft wings to achieve high strength in the top region and high damage tolerance in the lower region [2]. These specific properties are usually obtained by post-manufacture heat treatment. The mechanical properties achieved by WAAM aluminium material were investigated in numerous studies. Gu et al. [3] characterised the properties of as-deposited 2319 WAAM material. The authors showed that the relatively low mechanical properties in the as-deposited condition could be drastically improved by

heat treatment and inter-pass rolling. The authors also showed the effect of heat treatment and inter-pass rolling on 2319 alloy microstructure and porosity level and demonstrated the drastic porosity level reduction obtained by inter-pass rolling [4].

Considering how the WAAM process operates, a substrate is required as a base for starting the deposition. This substrate can be discarded or retained at the end of the component manufacture, depending on the final design. Several authors have reported the different advantages of keeping the substrate. Lockett et al. [5] provided an initial set of design rules for WAAM and showed that, in order to reduce the volume of deposited material and production time, the substrate often should be integrated into the final design. The final component would then be a hybrid mix of a wrought alloy on which the additive material has been deposited. Hybrid components, which are manufactured using a combination of conventional processes and an AM one, can benefit from the flexibility of AM without raising the manufacturing cost commonly associated with its low deposition rate. For instance, Ahuja et al. [6] showed the potential of hybrid manufacturing using laser beam melting and sheet forming to manufacture Ti6Al4V demonstrators. Additionally, Merklein et al. [7] demonstrated the possibility of combining several conventional processes with AM to produce functional gear components. In this case, they used a metal sheet as the substrate, powder-based fusion, laser cutting, deep drawing and upset forging to produce the component. The hybrid manufacturing route also allows the production of graded components using different materials for the substrate and filler wire with complementary and tailored properties. For example, Liu et al. [8] demonstrated the possibility of using a Laser-aided additive manufacturing process to produce sound structures made of cast iron substrate and Inconel 625 and stainless steel 420 deposits. Following this example, aluminium WAAM deposit could be combined with a rolled plate to manufacture functionality-graded components using different aluminium alloys for the wire and the plate. Several challenges must be tackled to use combinations of WAAM and wrought material: the deposition parameters should be optimised to reduce distortions and to residual stress of the substrate; the local microstructure and mechanical performances of the interface should be fully characterised.

There is a large amount of literature on WAAM, but relatively little is known about the properties of the interface between WAAM material and substrate. To the authors' knowledge, only two papers are focused on the matter: Zhang et al. [9] studied the fatigue behaviour of a Ti6Al4V interface; Gu et al. [10] investigated the deposition parameters' effect on the microstructure and tensile properties of aluminium interfaces. In this paper, the substrate and WAAM deposit were made of the same aluminium alloy. Therefore, the Interface between Substrate and the Deposited Metal (ISDM) of different aluminium alloys combination is the scope of this paper.

WAAM uses processes and consumables originally designed for welding. Therefore, the Interface between the Substrate and the Deposited Metal should perform suitably and in an equivalent manner in term of mechanical properties as traditionally observed in a welded structure. Numerous studies have been reported on the effect of fusion welding on aluminium. For example, Dumolt, Laughlin and Williams [11] investigated the effect of substrate temper on the microstructure of the Heat Affected Zone (HAZ) after welding using 2219 plates with the gas tungsten arc process. The substrate temper also affects the microstructure of the Partially Melted Zone (PMZ): Rao et al. [12] showed that the segregation of alloying elements, sometimes leading to liquation cracking, around the fusion zone can be affected by the substrate temper. The Fusion Zone (FZ) can be subject to hot cracking if the solidification behaviour of the mix of compositions of the substrate and wire alloys is not favourable. FZ hot cracking sensitivity has been widely studied: for instance, Pickin et al. [13] studied the effect of wire filler composition on multi-pass welding of 2024 plates. The authors used a tandem system to mix two aluminium wires of different grades to achieve tailored fusion zone chemical composition. They showed that the hot cracking tendency of 2024 alloy could be drastically reduced by using a suitable wire filler composition. Kou [14] used a different approach: the author built an index for predicting the susceptibility to solidification cracking of aluminium combinations during

welding. He showed that the use of suitable filler wires could drastically improve the solidification behaviour of the fusion zone, leading to crack free welds. All HAZ, PMZ and FZ can be found in the ISDM, as shown in Figure 1.

A considerable number of studies have been conducted on the additive manufacture of 2319 alloy [3,4,15–18]. This alloy is a conventional aluminium copper alloy which is widely applied as a welding wire in the aerospace and defence industries due to its favourable solidification behaviour and high strength after heat treatment. This alloy was therefore used in the present study. Four different alloys were used as substrates:

- The 2219 alloy is widely used as the structural alloy of cryogenic fuel tank of launch vehicles because of its mechanical properties and its fusion weldability with 2319 filler wire [19,20]. The 2219 alloy is very close to the 2319 alloy in composition except that 2319 alloy has a larger Titanium addition (Ti in 2219: 0.02–0.10%, 2319: 0.10%–0.20%)
- The 2024 alloy is used in the form of clad plates in aircraft fuselage [2]. It is considered unweldable by fusion processes because of its high susceptibility to liquation and hot cracking, especially when mixed with other alloys [13]. However, it has been shown by Pickin et al. that 2024 as a filler wire can be used to weld 2024 alloy plates [21].
- The 2050 alloy is an aluminium copper lithium alloy considered a medium- to high-strength alloy with high damage tolerance and corrosion resistance. The use of lithium significantly reduces the alloy density and this leads to a large weight saving ([22], Page 506). According to Lequeu et al., it can be used to replace 7000 series thick plates in aircraft internal structures [23]. However, cold work after solution treatment is needed to reach these high mechanical properties [24].
- The 2139 alloy is an aluminium copper magnesium silver alloy used in armoured vehicles manufacture [25]. In contrast to 2050 alloy, this alloy can attain high strength and damage tolerance without cold work thanks to homogeneously distributed precipitates. For this reason, the compatibility of this alloy with additive manufacturing has been investigated [26,27]. The authors used electron beam freeform fabrication and successfully deposited 2139 alloy. However, 2139 alloy was used only as a substrate in the study reported here.

In this paper, using microstructure analysis and micro hardness measurements, the ISDM properties in WAAM were investigated and compared to those seen between the weld and parent metal in conventional welding. The aim was to assess whether it is possible to achieve similar properties in the substrate and deposited material to achieve a homogenous structure. The results are organised separately according to the different areas of interest in the samples, shown in Figure 1.
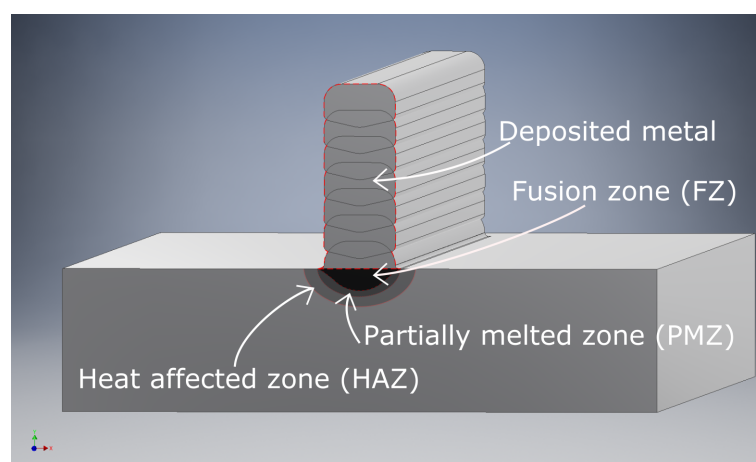

Figure 1. Areas of interest of the ISDM on a cross section perpendicular to the deposition direction.

2. Materials and Methods

2.1. Materials

Plates of the four alloys described in the introduction section (2219, 2024, 2050 and 2139) were machined and cut to 100 mm × 400 mm × 12 mm substrates. The tempers and chemical compositions of the plates and wire are given in Table 1.

Table 1. Composition of the alloys used as wire and substrates. The chemical composition of the wire was measured using Energy Dispersive X-ray Spectroscopy, and the chemical composition of the substrates was provided by the Aluminium Association [28].

Alloy	Temper	Cu	Mn	Mg	Ag	Li
2319 (wire)	-	6.04 ± 0.06	0.27 ± 0.02	0.03 ± 0.01	-	-
2219 (substrate)	T8	5.8–6.8	0.20–0.40	0.02	-	-
2024 (substrate)	T3	3.8–4.9	0.30–0.9	1.2–1.8	-	-
2139 (substrate)	T3	4.5–5.5	0.20–0.6	0.20–0.8	0.15–0.6	-
2050 (substrate)	T3	3.2–3.9	0.20–0.50	0.20–0.6	0.20–0.7	0.7–1.3

2.2. Experimental Procedure

Seven-layer high and 380 mm long walls were deposited on the centre of the plates using stringer beads and the deposition parameters shown in Table 2. An ABB 6 axis robot and a Fronius CMT Advanced 4000R machine were used as manipulator and power source, respectively. The waiting time between layers was set to two minutes. The main process used was Cold Metal Transfer Pulse Advanced (CMT-PA, synergic line C1369) due to its capability to produce low-porosity Al–Cu deposits [29]. As detailed by Gierth et al. [30], the deposition parameters used for the wall base need to be changed to adapt to the change of heat flux to produce walls of constant width. CMT-PA is a very low heat input process and is not suitable to deposit the first layer. Therefore, the CMT pulse process (synergic line C0880), a higher heat input mode, was used to deposit the first layer. For subsequent layers, CMT-PA was used with a wire feed speed decreasing from the third to the sixth layer. Consequently, heat input was reduced as the wall height increases, keeping the thermal cycle relatively constant in the deposited material. The distance between the torch and the work-piece and the travel speed were kept at constant 11 mm and 10 mm/s, respectively.

Table 2. Deposition parameters.

Layer	Wire Feed Speed	Process	Travel Speed	Contact Tip to Work-Piece Distance
1	7 m/min	CMT Pulse		
2, 3	9 m/min			
4, 5	7 m/min	CMT Pulse Advanced	10 mm/s	11 mm
6, 7	6 m/min			

The cross sections of interfaces were cut; mounted in cold epoxy resin; and ground with 240, 600, 1200 and 2500 grit SiC papers with flowing water as the coolant to avoid any rise in material temperature, which might affect the strength. Finally, the samples were polished to a mirror finished using a 3 μm diamond paste and colloidal suspension solution for microstructure analysis.

The heat treatment, designed for 2319 alloy, to T6 temper was carried out in a furnace chamber. During solution treatment, the samples were heated from room temperature to 507 °C at 40 °C/h and then heated up to 534 °C at 20 °C/h. Heating was carried out in two steps to avoid any temperature overshoot near the melting point of 2319 alloy. It needs to be highlighted here that the solution treatment temperature was selected for the 2319 WAAM deposited alloy without taking into consideration the melting points of the substrates. In the case of the 2024 substrate, partial melting is bound to happen at 534 °C as 2024 alloy melting point is 504 °C, considerably lower than the melting point of 2319 alloy

at 543 °C. These samples were kept at 534 °C for two hours before being water quenched. Finally, the samples were aged at 171 °C for 14 h.

A Nikon Optiphot 2 microscope was used to capture the optical images, and Scanning Electron Microscopy was performed using an Tescan Vega 3 machine. The samples were coated with a 10 nm layer of gold before SEM observation. An INCAx-act detector was used to measure local chemical composition. Three measurements were carried out in the fusion zone and the first layer of deposited material of each sample.

To evaluate the dimension and mechanical properties of the HAZ, hardness measurements were performed in the transverse cross-sectional plane 1 mm below the substrate top surface, as shown by the path A in Figure 2. These measurements were performed on one sample per alloy combination using a Vickers micro hardness testing machine (Auto-C.A.M.S. of Zwick Roell) with a load of 100 g and a duration of 15 s.
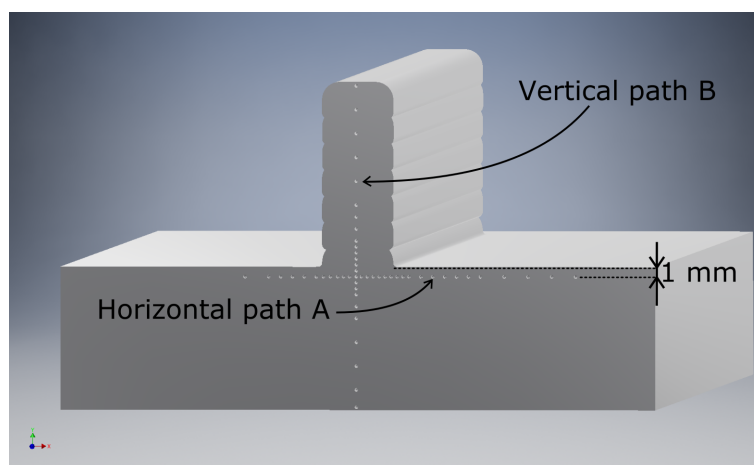

Figure 2. Scheme of the horizontal (A) and vertical (B) hardness path.

In the PMZ, the peak temperature reached was above the melting point of the solute atoms on and along the grain boundaries. This zone was characterised by the presence of liquations, and its width was measured on SEM images using the Axiovision software.

The FZ and deposited material were characterised by the hardness profile measured along a vertical path in the centre of the deposited material, as shown in Figure 2 path B, using the same testing parameters as for the HAZ.

3. Results

3.1. Substrate

3.1.1. As-Deposited Hardness Profile

Horizontal hardness profiles before and after heat treatment are shown for each alloy combination in Figure 3. For all cases, the minimum hardness occurred in the FZ. For the 2219 substrate, the hardness increased smoothly across the HAZ and stabilised 8 mm away from the deposition centreline. In contrast, for the other substrates, there was a sharp hardness change between the FZ and the HAZ. Additionally, a drop in hardness was measured further away inside the HAZ: for the 2024 and 2139 substrate, hardness decreases by 20 to 30% of the base plate value at 8 mm from the centreline. For the 2050 substrate, there was a similar drop but 14 mm away from the centreline.
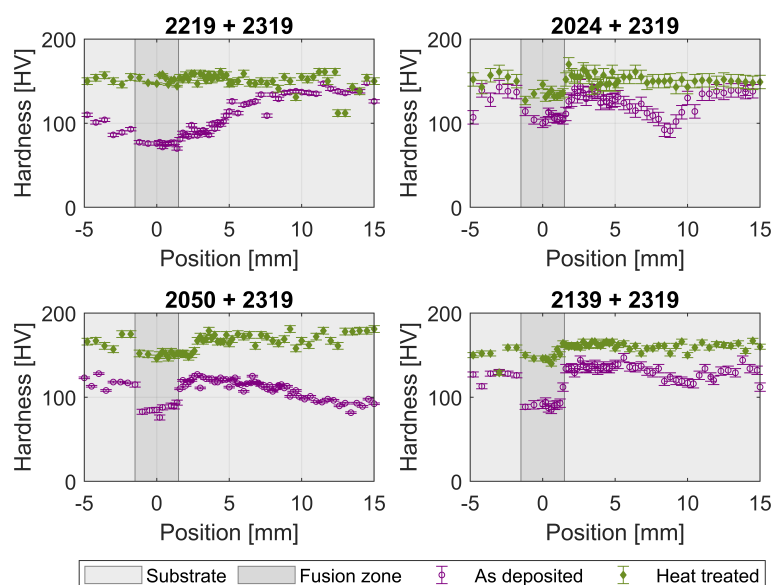
Figure 3. Hardness profile of the heat affected zone, measured 1 mm under the substrate top surface.

3.1.2. Hardness Profile after Heat Treatment

The hardness profiles after heat treatment are also shown in Figure 3. The hardness in the substrate depended on its composition. In terms of profile, the hardness was constant along the entire path when the substrate was made of 2219, but when 2024, 2050 or 2139 substrates were used, a net drop was observed at the centre of the deposition line. Nevertheless, the difference between the fusion zone and the parent material was reduced compared to the as-deposited condition. For instance, the hardness dropped by 33% between the fusion zone and the parent metal in the 2139 substrate before heat treatment while it only dropped by 10% in the T6 condition.

3.1.3. As-Deposited Microstructure

As shown in Figure 4, no cracks were found in optical images of the ISDM with 2219, 2024 and 2050 substrates. However, a crack was found in the 2139 substrates. The crack, magnified in the inset Figure 4d, propagated from the edge of the deposit in the grain boundary and started at the edge of the FZ.
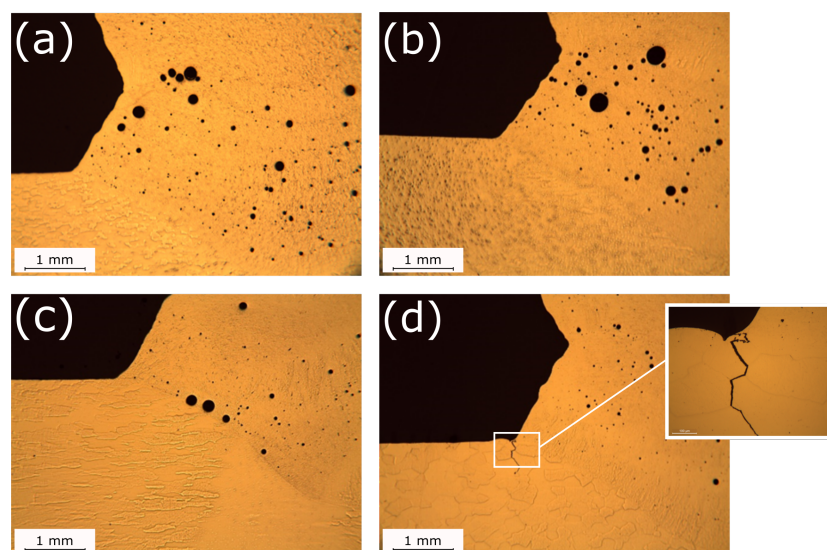

Figure 4. Optical image of cross sections focused on the FZ/PMZ boundary in the (**a**) 2219, (**b**) 2024, (**c**) 2050 and (**d**) 2139 substrates.

Figure 5 shows that liquations were observed at the grain boundaries in the PMZ of the samples built for this study, regardless of the substrate alloy or temper used. However, as shown in Figure 6, the width of the zone affected by liquation changed with the substrate: 200 μm for the 2219, 2024 and 2050 substrates and 480 μm wide in case of the 2139 substrate.
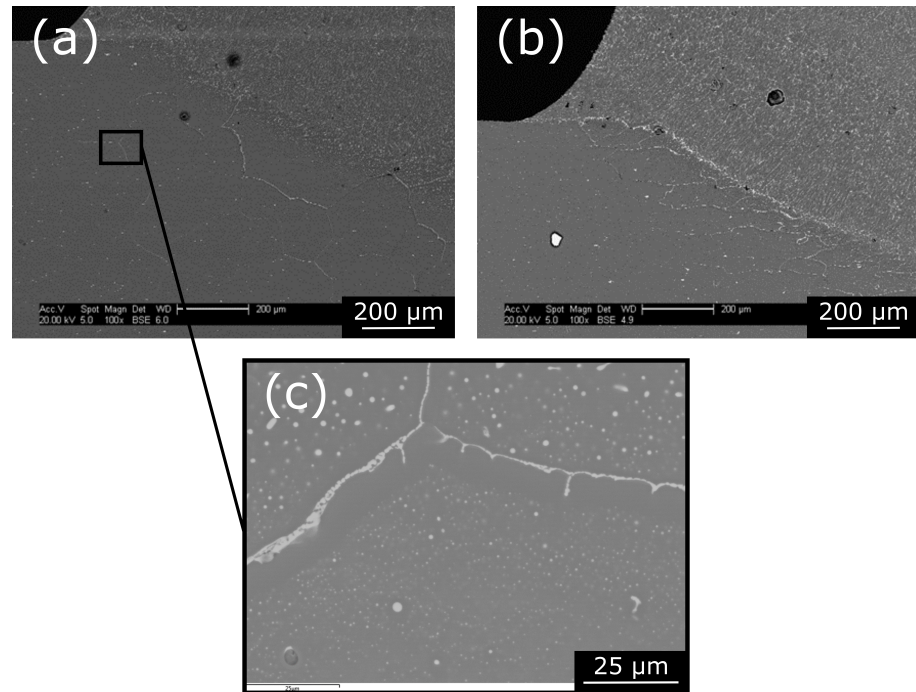

Figure 5. SEM images of the PMZ in the (**a**) 2139 and (**b**) 2050 substrates at low magnification and in the (**c**) 2139 substrate at higher magnification.
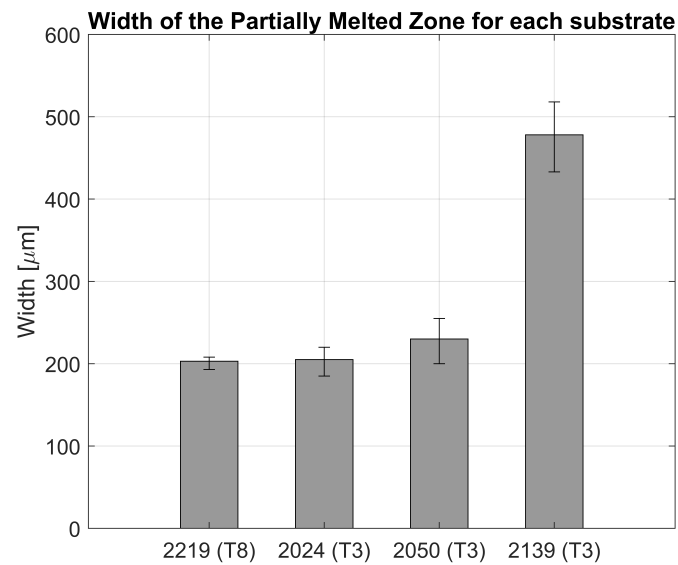

Figure 6. Width of the area affected by liquation depending on the substrate used.

3.1.4. Microstructure after Heat Treatment

After heat treatment, liquation was not observed anymore in the 2219 and 2050 samples, as illustrated in Figures 7 and 8 in (b) and (f). However, images (d) and (h) show that this area was severely affected by grain boundary cracks at grain boundaries in the 2024 and 2139 substrates.
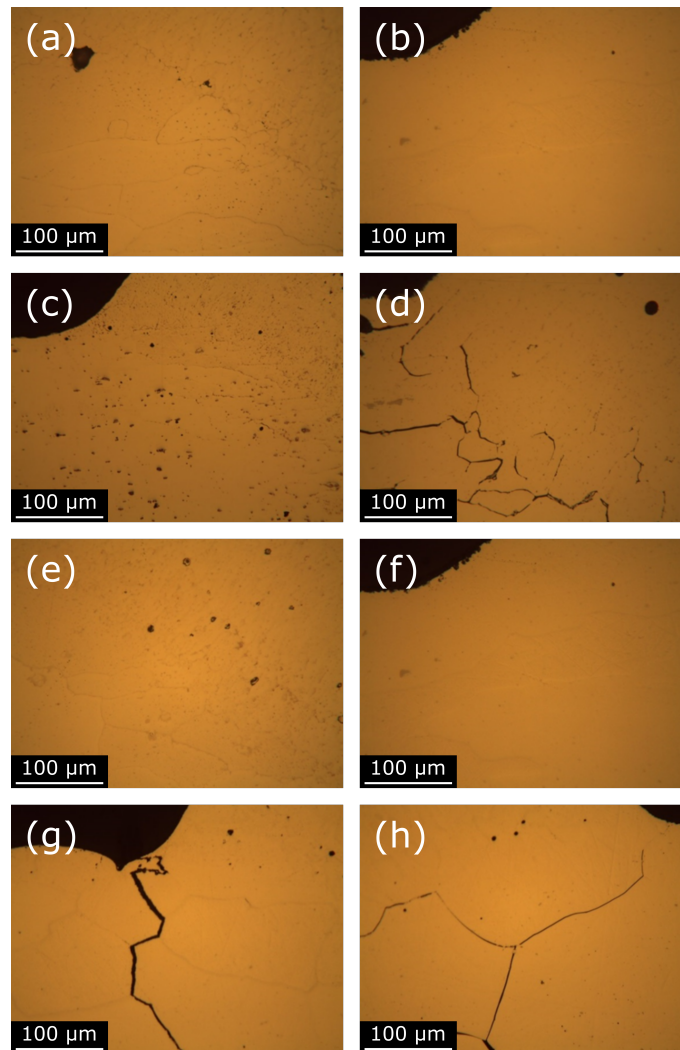

Figure 7. Optical images of ISDM before (left column) and after (right column) heat treatment for the four configurations with the (**a**,**b**) 2219, (**c**,**d**) 2024, (**e**,**f**) 2050 and (**g**,**h**) 2139 substrates.
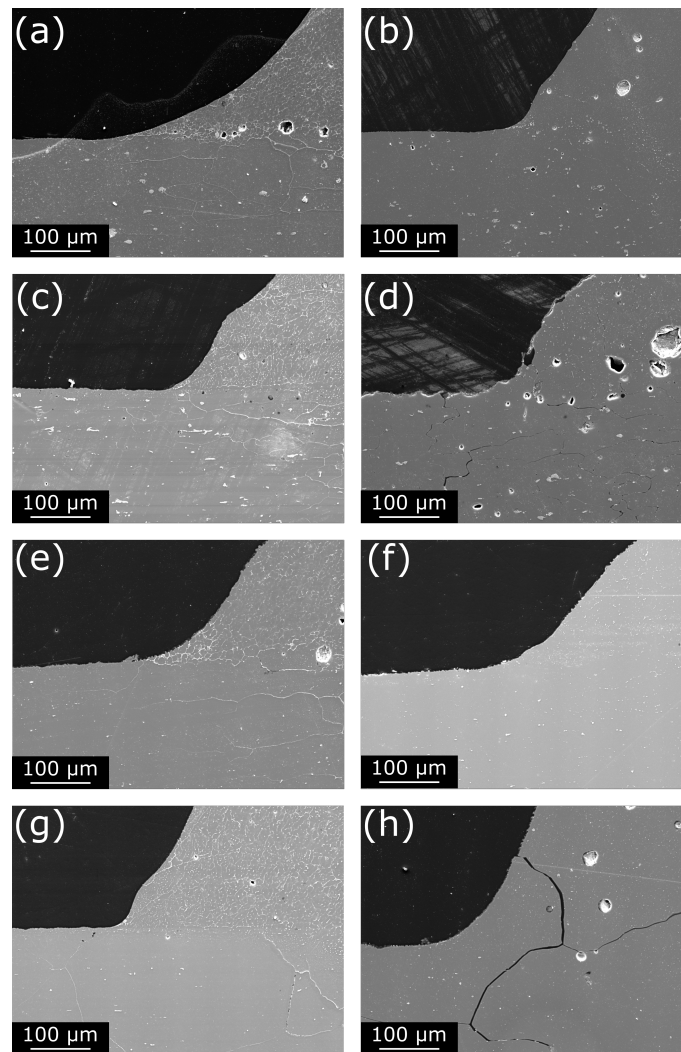
Figure 8. SEM images of ISDM before (left column) and after (right column) heat treatment for the four configurations with the (**a**,**b**) 2219, (**c**,**d**) 2024, (**e**,**f**) 2050 and (**g**,**h**) 2139 substrates.

3.2. Fusion Zone and Deposited Material

3.2.1. Porosity

Figure 4 shows optical images of the fusion zone: porosity is visible in all of the combinations, regardless of the substrate alloy. Porosity in the 2319 alloy deposited by WAAM has been studied previously by Gu et al. [3] and Cong et al. [29], and it will not be discussed further here.

3.2.2. Hardness Profile

The hardness profiles of the ISDMs, measured along the scan line B shown in Figure 2, are shown in Figure 9. The hardness values reached in the substrate, fusion zone and deposited material are given in Table 3.
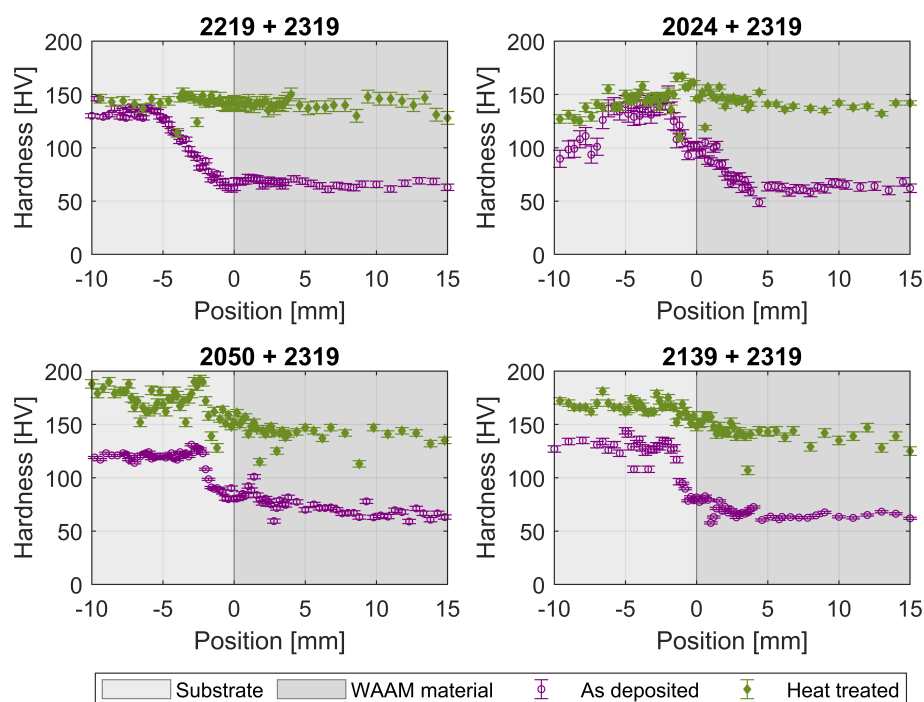
Figure 9. Vertical hardness profile before and after heat treatment for each alloy combination.

Table 3. Average of the Vickers hardness values measured in the three areas of interest before and after heat treatment.

Sample	Substrate Alloy	2219	2024	2139	2050
	Substrate	133 ± 2	119 ± 7	130 ± 3	120 ± 2
As-deposited	Fusion zone	68 ± 2	99 ± 5	79 ± 5	86 ± 4
	Deposited material	66 ± 1	62 ± 4	65 ± 1	67 ± 2
	Substrate	142 ± 4	136 ± 4	169 ± 3	172 ± 4
Heat treated	Fusion zone	142 ± 1	149 ± 2	154 ± 3	151 ± 4
	Deposited material	141 ± 2	141 ± 2	136 ± 4	138 ± 3

In the as-deposited condition, the hardness measured in the deposited material was lower than in the substrate regardless of the composition of the substrate; 5 mm away from the substrate top surface, the deposited metal hardness did not depend on the substrate and is equal to 65 HV.

When the deposition was onto 2219 substrate, the transition between the substrate and the fusion zone was smooth; the minimum hardness was reached in the fusion zone and was constant in the deposited material. Regarding substrates 2024, 2050 and 2139, there were two sharp drops of hardness, first at the fusion line at about 2 mm deep in the substrate and then at about 1 mm high in the deposited material. Additionally, a reduction of hardness was noticeable 6 mm deep in the 2024 substrate.

After heat treatment, the deposited material reached a constant hardness of about 140 HV regardless of what substrate was used. In the case of the 2219 substrate, the hardnesses were even across the interface. For the 2050 and 2139 substrates, all substrates, FZ and deposited material hardnesses increased after heat treatment, and the difference between the substrate and the deposited material hardness was reduced. For 2024, the drop in hardness in the HAZ was reduced, but there was no significant hardness increase in the substrate. The profile of hardness was almost even, with a peak in the fusion zone.

Figure 10 shows the magnesium and copper content across the four interfaces. The chemical compositions of the substrate provided at the position −4 mm are the registered composition of the alloy used [28]. When the 2219 substrate was used, no variation in

copper and magnesium content was observed across the interface. However, the chemical composition of the FZ differed from that of the WAAM material and substrate in the other three cases.
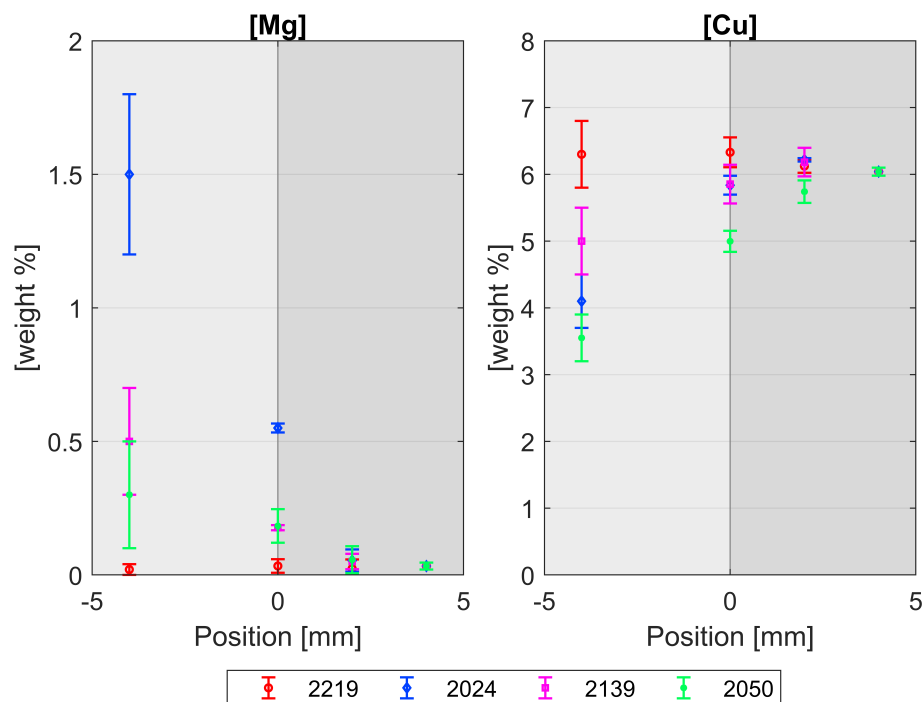

Figure 10. Magnesium and copper contents across the interfaces.

4. Discussion

4.1. Substrate

4.1.1. As-Deposited Hardness Profile

Two factors make 2219 different from the other three substrates in this study: the composition and the temper. First, the 2219 substrate composition is very close to the 2319 alloy wire. Therefore, there is no composition difference between the FZ and the HAZ. This is the first reason why there is no steep hardness drop at the boundary between those two areas. This is explained further in the paragraph related to the deposited material study in Section 4.2. Second, the 2219 plate is artificially aged while the other three were in naturally aged condition before deposition. As a result, the microstructure of the HAZ is different. The effect of pre-deposition base plate temper has been widely studied in aluminium fusion welding [11,12,31]. When the base metal is naturally aged and contains Guinier–Preston zones, the post welded plate presents a softened area situated a few millimetres from the fusion zone where coarser phases are generated during the heat cycle. That is why a drop in hardness was observed in the plates 8 to 13 mm away from the deposition in the three naturally aged substrates.

4.1.2. Hardness Profile after Heat Treatment

The 2219 substrate recovers during the heat treatment as the compositions of the FZ and HAZ are the same and respond in a similar manner to heat treatment. Unlike the FZ and HAZ in the 2219 substrate, 2024, 2139 and 2050 FZ and HAZ have different compositions and that is why the hardness was not the same in those areas after heat treatment. For the 2139 and 2050 alloys, there was a net increase in hardness in the substrate, while the 2024 hardness remained the same. For the latter, this is due to the low ageing kinetic of the 2024 alloy. This alloy requires a higher ageing temperature than other 2xxx series alloys as shown by the typical heat treatment duration and temperature reported by [32]. The ageing treatment carried out in this study was about 20 °C too low to have a considerable effect on this substrate.

4.1.3. As-Deposited Microstructure

Hot cracking is a common problem in fusion welding of aluminium, especially for aluminium copper alloys, such as 2024, 2139 and 2050, which were used in this study. The 2219 alloy is one of the few alloys considered weldable from the 2000 series. However, no cracks were found in the 2024 and 2050 substrate after deposition. Additive manufacturing differs from welding in several ways. In welding, two plates are joined together and many different edge preparations and mating face configurations exist. In comparison, in additive manufacturing, a metal bead is deposited on a plate or previously deposited beads. The objectives are different in term of bead shape: in welding, significant penetration is generally required to ensure good joint properties; in additive manufacturing, the aim is to add material so that penetration tends to be reduced as much as possible. Constraint during welding is much higher compared to additive manufacturing, which by its very nature is free-form, and therefore, restraint acting on the melt pool and in the solidifying region is much less. Furthermore, the stress generated during solidification is the main cause of hot cracking during fusion welding. This explains why solidification cracks were not observed in both optical and SEM images of as-deposited samples in this study, even when 2024 and 2050 alloys were used.

As demonstrated in the literature [33–35], even if hot cracks are avoided, the mechanical properties of PMZ tend to be reduced by liquation. That is why the size of the area affected by liquation is of interest. This area was about twice as large in the 2139 substrate compared to in the other three base plates. This observation shows the effect of grain size on liquation: the bigger the grains, the wider the area affected by liquation. A similar conclusion has been made in fusion welding by Rao et al. [12]. Therefore, reducing the substrate grain size might be a way to improve the as-deposited mechanical properties of the IDSM. The formation of liquation cracks also depend upon the orientation of the grain boundaries and the stress generation. Nonetheless, composition and thermal conductivity are probably critical factors regarding liquation along with grain size.

4.1.4. Microstructure after Heat Treatment

During solutionising, the eutectic compound solutionises and forms a single phase with the aluminium matrix. This phenomenon is visible on the ISDM with 2050 and 2219 pictures (b) and (f) in Figure 7: the composition became homogeneous, and grain boundary segregation was highly reduced. However, one of the main challenges of building and heat treating dissimilar alloy parts is the incompatibility of their respective conventional heat treatment: in the case of the ISDM with 2024 and 2139, cracks were generated along the liquation zone during solution treatment (Figure 7). The origin of these cracks is not the same for both cases. For 2024 substrate, the solution treatment temperature adopted for the deposited 2319 alloy was too high for 2024: its melting point is 504 °C, and the temperature reached during the heat treatment was 535 °C. This means that the eutectic compound was melted during the soaking. The molten grain boundary could not sustain the stress generated by the surrounding solid during the quench: this led to solidification cracks forming. To heat treat this combination, a lower temperature solution treatment could be used, but this treatment would not be effective to solutionise the 2319 WAAM material. This illustrates the challenges in tackling heat treatment of a dissimilar alloy component. For 2139 substrate, the solution treatment temperature was not higher than the eutectic melting point, but the fast cooling occurring during the quench probably generated stresses helping the propagation of cracks along grain boundaries, weakened by microcracks generated during deposition. The grain boundaries are weakened during deposition as low temperature eutectic formed by segregation along them later melts and opens up under stress.

4.2. Fusion Zone and Deposited Material

4.2.1. As-Deposited

When the 2319 alloy was deposited onto the 2219 substrate, there was no significant change in the composition along the deposit as the composition of the deposit and parent

material were essentially the same. This explains the constant value of hardness in the deposited material when the 2219 substrate was used. The smooth reduction of hardness change can be attributed to the peak aged state of the substrate before deposition (T8 temper); similar observations have been made in fusion welding [11].

For the other three substrates, the wire composition differed from that of the substrate. Therefore, there was a mix of alloying elements and the composition changed across the first and second layers, as shown in Figure 10. This dilution explains the plateau of hardness observed in the fusion zone in the three 2024, 2050 and 2139 alloys.

The drop in hardness observed in the 2024 substrate 6 mm deep in the substrate was the same drop as observed in the horizontal hardness measurement at about 8 mm away from the deposition centreline. It was due to the precipitation of a band of θ' phases in the heat affected zone, lowering the hardness as detailed in the literature [11,31]. As shown in Figure 3, this drop in hardness was more significant for 2024, and this is why it was noticeable only for this alloy on the vertical hardness path in Figure 9.

4.2.2. After Heat Treatment

For the 2219 substrate, the hardness profile was even: this is because the composition of the substrate, FZ and deposited material were the same, so the response toward heat treatment was the same in term of hardness increase.

For the 2139, 2024 and 2050 substrates, the smooth drop in hardness between the substrate and deposited material was due to the change of composition at the interface and the different response toward heat treatment of those compositions.

5. Conclusions

This study shows that the Interface between Substrate and the Deposited Material includes a fusion zone, partially melted zone and heat affected zone just as in the interface between parent material and the weld bead in fusion welding. However, the stresses generated during WAAM are lower than during welding, and this can enable the use of alloys considered unweldable as WAAM substrate. The effect of both substrate alloy and temper were studied: the results highlight that the substrate needs to be carefully selected when manufacturing a component. Its composition needs to be compatible with the deposited alloy if a heat treatment needs to be carried out after the manufacture, and its temper needs to be suitable if no heat treatment is conducted.

Using the 2319 alloy as a filler wire, it was not possible in this study to achieve homogeneous hardness across the interface without post-deposition heat treatment. The combination using 2219 and 2050 substrates were both successfully heat-treated, but only the interface between the 2219 substrate and WAAM material reached homogenous hardness. Therefore, this combination would be the simplest to use, but the design advantages of using different alloy for the substrate and filler wire remained to be explored.

For optimal performances, substrates should be specially manufactured to suit the WAAM process to reduce the risk of liquation cracking or a coarse change in properties and to adapt to the deposited alloy to avoid hot cracking and to match with the heat treatment of the deposited material. Further work needs to be carried out to assess the effect of the ISDM microstructure on the static and dynamic mechanical behaviours of the join between WAAM material and substrate.

Data Availability Statement: The data underlying this study can be accessed through the Cranfield University repository at https://doi.org/10.17862/cranfield.rd.12497006.

Conflicts of Interest: The authors declare no conflict of interest.

References

1. Williams, S.W.; Martina, F.; Addison, A.C.; Ding, J.; Pardal, G.; Colegrove, P. Wire+Arc Additive Manufacturing. *Mater. Sci. Technol.* **2016**, *32*, 641–647. [CrossRef]
2. Starke, E.; Staley, J. Application of modern aluminum alloys to aircraft. *Prog. Aerosp. Sci.* **1996**, *32*, 131–172. [CrossRef]
3. Gu, J.; Ding, J.; Williams, S.W.; Gu, H.; Ma, P.; Zhai, Y. The effect of inter-layer cold working and post-deposition heat treatment on porosity in additively manufactured aluminum alloys. *J. Mater. Process. Technol.* **2016**, *230*, 26–34. [CrossRef]
4. Gu, J.; Ding, J.; Williams, S.W.; Gu, H.; Bai, J.; Zhai, Y.; Ma, P. The strengthening effect of inter-layer cold working and post-deposition heat treatment on the additively manufactured Al–6.3Cu alloy. *J. Mater. Process. Technol.* **2016**, *651*, 18–26. [CrossRef]
5. Lockett, H.; Ding, J.; Williams, S.; Martina, F. Design for Wire + Arc Additive Manufacture: Design rules and build orientation selection. *J. Eng. Des.* **2017**, *28*, 568–598. [CrossRef]
6. Ahuja, B.; Schaub, A.; Karg, M.; Schmidt, R.; Merklein, M.; Schmidt, M. High power laser beam melting of Ti 6 Al 4 V on formed sheet metal to achieve hybrid structures. *Laser 3D Manuf. II* **2015**, *9353*, 93530X. [CrossRef]
7. Merklein, M.; Schulte, R.; Papke, T. An innovative process combination of additive manufacturing and sheet bulk metal forming for manufacturing a functional hybrid part. *J. Mater. Process. Technol.* **2021**, *291*, 117032. [CrossRef]
8. Liu, Y.; Weng, F.; Bi, G.; Chew, Y.; Liu, S.; Ma, G.; Moon, S.K. Characterization of wear properties of the functionally graded material deposited on cast iron by laser-aided additive manufacturing. *Int. J. Adv. Manuf. Technol.* **2019**, *105*, 4097–4105. [CrossRef]
9. Zhang, J.; Zhang, X.; Wang, X.; Ding, J.; Traoré, Y.; Paddea, S.; Williams, S. Crack path selection at the interface of wrought and wire + arc additive manufactured Ti–6Al–4V. *Mater. Des.* **2016**, *104*, 365–375. [CrossRef]
10. Gu, J.; Yang, S.; Gao, M.; Bai, J.; Liu, K. Influence of deposition strategy of structural interface on microstructures and mechanical properties of additively manufactured Al alloy. *Addit. Manuf.* **2020**, *34*, 101370. [CrossRef]
11. Dumolt, S.D.; Laughlin, D.E.; Williams, J.C. The Effect of Welding on the Microstructure of the Age Hardening Aluminum Alloy 2219. In Proceedings of the First International Aluminum Welding Conference, Cleveland, OH, USA, 1981; pp. 115–135. Available online: https://www.andrew.cmu.edu/user/dl0p/laughlin/pdf/030.pdf (accessed on 1 October 2018).
12. Rao, K.S.; Reddy, G.M.; Rao, K.P. Studies on partially melted zone in aluminium-copper alloy welds—Effect of techniques and prior thermal temper. *Mater. Sci. Eng. A* **2005**, *403*, 69–76. [CrossRef]
13. Pickin, C.G.; Williams, S.W.; Prangnell, P.B.; Robson, J.; Lunt, M. Control of weld composition when welding high strength aluminium alloy using the tandem process. *Sci. Technol. Weld. Join.* **2009**, *14*, 734–739. [CrossRef]
14. Kou, S. A Simple Index for Predicting the Susceptibility to Solidification Cracking. *Weld. J.* **2015**, *94*, 374–388.
15. Ayarkwa, K.F.; Williams, S.; Ding, J. Investigation of pulse advance cold metal transfer on aluminium wire arc additive manufacturing. *Int. J. Rapid Manuf.* **2015**, *5*, 44–57. [CrossRef]
16. Bai, J.Y.; Yang, C.L.; Lin, S.B.; Dong, B.L.; Fan, C.L. Mechanical properties of 2219-Al components produced by additive manufacturing with TIG. *Int. J. Adv. Manuf. Technol.* **2015**, *86*, 479–485. [CrossRef]
17. Ryan, E.M.; Sabin, T.J.; Watts, J.F.; Whiting, M.J. The influence of build parameters and wire batch on porosity of wire and arc additive manufactured aluminium alloy 2319. *J. Mater. Process. Technol.* **2018**, *262*, 577–584. [CrossRef]
18. Cong, B.; Qi, Z.; Qi, B.; Sun, H.; Zhao, G.; Ding, J. A Comparative Study of Additively Manufactured Thin Wall and Block Structure with Al-6.3%Cu Alloy Using Cold Metal Transfer Process. *Appl. Sci.* **2017**, *7*, 275. [CrossRef]
19. Li, Q.; Wu, A.; Li, Y.; Wang, G.; Yan, D.; Liu, J. Influence of temperature cycles on the microstructures and mechanical properties of the partially melted zone in the fusion welded joints of 2219 aluminum alloy. *Mater. Sci. Eng. A* **2015**, *623*, 38–48. [CrossRef]
20. Sasabe, S. Weld cracking and joint strength of 2219 by MIG welding. *Weld. Int.* **2015**, *48*, 23–32. [CrossRef]
21. Pickin, C.G.; Williams, S.W.; Prangnell, P.B.; Robson, J.; Lunt, M.; Derry, C.; Lunt, M. Control of weld composition when arc welding high strength aluminium alloys using multiple filler wires. *Sci. Technol. Weld. Join.* **2010**, *15*, 491–496. [CrossRef]
22. Prasad, N.E.; Gokhale, A.A.; Wanhill, R.J.H. *Aluminum-Lithium Alloys: Processing, Properties, and Applications*; Elsevier: Amsterdam, The Netherlands, 2014.
23. Lequeu, P.; Smith, K.P.; Daniélou, A. Aluminum-Copper-Lithium Alloy 2050 Developed for Medium to Thick Plate. *J. Mater. Eng. Perform.* **2010**, *19*, 841–847. [CrossRef]
24. Gable, B.M.; Zhu, A.W.; Csontos, A.A.; Starke, E.A. The role of plastic deformation on the competitive microstructural evolution and mechanical properties of a novel Al-Li-Cu-X alloy. *J. Light Met.* **2001**, *1*, 1–14. [CrossRef]
25. Kozmel, T.; Vural, M.; Tin, S. EBSD analysis of high strain rate application Al–Cu based alloys. *Mater. Sci. Eng. A* **2015**, *630*, 99–106. [CrossRef]
26. Brice, C.; Shenoy, R.; Kral, M.; Buchannan, K. Precipitation behavior of aluminum alloy 2139 fabricated using additive manufacturing. *Mater. Sci. Eng. A* **2015**, *648*, 9–14. [CrossRef]
27. Brice, C.A.; Tayon, W.A.; Newman, J.A.; Kral, M.V.; Bishop, C.; Sokolova, A. Effect of compositional changes on microstructure in additively manufactured aluminum alloy 2139. *Mater. Charact.* **2018**, *143*, 50–58. [CrossRef]

28. The Aluminum Association Inc. *International Alloy Designations and Chemical Composition Limits for Wrought Aluminum and Wrought Aluminum Alloys*; The Aluminum Association: Arlington, TX, USA, 2009.
29. Cong, B.; Ding, J.; Williams, S.W. Effect of arc mode in cold metal transfer process on porosity of additively manufactured Al-6.3%Cu alloy. *Int. J. Adv. Manuf. Technol.* **2014**, *76*, 1593–1606. [CrossRef]
30. Gierth, M.; Henckell, P.; Ali, Y.; Scholl, J.; Bergmann, J.P. Wire Arc Additive Manufacturing (WAAM) of Aluminum Alloy AlMg5Mn with Energy-Reduced Gas Metal Arc Welding (GMAW). *Metals* **2020**, *13*, 2671. [CrossRef]
31. Kou, S. Precipitation-Hardening Materials I: Aluminium Alloys. In *Welding Metallurgy*, 2nd ed.; John Wiley & Sons, Inc.: Hoboken, NJ, USA, 2003; Chapter 15, pp. 353–374.
32. Davis, J. Heat Treating of Aluminum alloys. In *Aluminum and Aluminum Alloys*, 2nd ed.; ASM International: Novelty, OH, USA, 1998; Section 7, pp. 1032–1039.
33. Huang, C.; Cao, G.; Kou, S. Liquation cracking in partial penetration aluminium welds: Assessing tendencies to liquate, crack and backfill. *Sci. Technol. Weld. Join.* **2004**, *9*, 149–156. [CrossRef]
34. Huang, C.; Kou, S. Partially Melted Zone in Aluminum Welds—Liquation Mechanism and Directional Solidification. *Weld. Res.* **2000**, *79*, 113–120.
35. Huang, C.; Kou, S. Liquation mechanisms in multicomponent aluminum alloys during welding. *Weld. Res.* **2002**, *81*, 211–222.

Short Biography of Authors

Eloise Eimer is a research fellow of the Welding Engineering and Laser Processing Centre at Cranfield University, UK. She obtained her PhD degree in 2019 in the same research department. She previously worked on aluminium semi-finished product manufacture, and her main research areas are alloy and process development for aluminium Wire + Arc Additive Manufacture.

Stewart Williams is a Professor and the Director of the Welding Engineering and Laser Processing Centre at Cranfield University, UK. His main research interests lie in application of high deposition additive manufacture, weld process and additive manufacture modelling, lasers in material processing and stress engineering.

Jialuo Ding is a Principal Research fellow of the Welding Engineering and Laser Processing Centre at Cranfield University, UK. Her main research areas are thermal-mechanical simulation of the WAAM process, WAAM process development of different materials and WAAM process automation and control.

Supriyo Ganguly is a Reader in Welding and Additive Materials Science in the Welding Engineering and Laser Processing Centre and also the Director of the Masters in Welding Science course at the Cranfield University. Supriyo is a Material Scientist and presently his research is focussed on understanding response of different structural alloys to transient thermal cycles during advanced and high-power density fabrication and processing and its impact on the integrity of a structure. He has about 85 peer reviewed publications in the areas of material processing, wire plus arc additive manufacture and integrity of structural alloys.

Bechir Chehab is a Technical Project Leader at Constellium Technology Center in charge of aluminium alloy development for additive manufacturing applications. His main research areas are: aluminium alloys design, development of new aluminium multilayer brazing sheets, continuous casting of stainless steels, compositionally graded steels.

2021-06-04

Effect of substrate alloy type on the microstructure of the substrate and deposited material interface in aluminium wire + arc additive manufacturing

Eimer, Eloise